Dynamics of premelted films: Frost heave in a capillary

J. S. Wettlaufer
Applied Physics Laboratory HN-10, University of Washington, Seattle, Washington 98105

M. G. Worster
Institute of Theoretical Geophysics, Department of Applied Mathematics and Theoretical Physics, University of Cambridge, CB3 9EW Cambridge, England

(Received 27 May 1994)

Due either to van der Waals or to short range interactions, some materials will interfacially premelt against a foreign substrate. We present a theoretical study of this phenomenon for a situation in which the material is confined within a deformable capillary tube. At a temperature below the bulk melting transition an annulus of premelted liquid separates the solid from the capillary walls. For an isothermal capillary, at finite reduced temperature, the film is of uniform thickness and is static. On imposition of an axial temperature gradient the thickness of the film varies with position along the axis. A thermomolecular pressure gradient transports fluid towards regions of colder temperatures, where it solidifies and deforms the confining capillary. For the case of van der Waals interactions we formulate a mathematical model and solve it numerically and by matched asymptotic expansions. The main result is the temporal and spatial deformation of the capillary tube; a measurable quantity. In the case of a transient thermal field, we find that the deformation of the capillary is small and that it is uniform over most of its length. For a steady thermal field, large deformation occurs in a region of small reduced temperature and grows towards the cold end of the capillary. We focus on ice monocrystals, and offer our theory as a model for frost-heave phenomena, with the advantage of having exposed the essential physics of the problem in the absence of impurity and curvature effects. The experiments conducted by Wilen and Dash [Bull. Am. Phys. Soc. **38**, 747 (1993); Phys. Rev. Lett. (to be published)] provide information that is unavailable using equilibrium techniques, and form the relevant test of this theoretical approach.

PACS number(s): 68.45.Gd, 68.55.Jk, 68.35.Rh

I. INTRODUCTION

A. Statics

The interface between a foreign substrate and a solid, or a grain boundary between two crystals, may be wetted by a thin liquid film formed from the solid. When the film persists at temperatures below the bulk melting transition of the solid, the phenomenon is termed *interfacial melting*, and it is theoretically analogous to other wetting transitions [1,2]. The problem holds the attention of condensed matter scientists both because of its basic significance as a surface phase transition, and for its broad technical applicability, biological relevance, and environmental consequences [3].

From the perspective of physical adsorption, wetting on a planar, nonreactive substrate has a well developed theoretical foundation [1]. There is active interest in the adsorption of films and/or the wetting of binary liquid mixtures on substrates with nonplanar geometries such as in wedges [4] and pores [5,6]. While the theoretical techniques vary from microscopic to macroscopic, such studies focus on understanding *states* which characterize thermodynamic *equilibrium*. Examples of the results of such studies include the thickness and variation of the film density normal to an interface, the excess coverage in a wedge, and the domain geometries of phase-separated two-component fluids, and how these vary with the intensive parameters and the interfacial interaction potentials. When the film in question has a density that departs significantly from that of the bulk fluid, due to confining effects, say, then microscopic treatments are necessary. Dietrich [7] reviews the concept of an effective interface potential and its application to the formation of thin one- and two-component films, and Evans [5] gives a thorough review of the equilibrium properties of one-component fluids confined in idealized slits and pores.

The extension of a region of coexistence to temperatures below bulk equilibrium indicates the presence of a thermomolecular pressure in a material [8]. As a result, interfacial melting can occur. Experimental evidence has been found for ^{4}He in Vycor glass [3], for ice in graphite powder and exfoliated graphite crystals [9], for ice in polyethylene and silica powders and mineral soils [10], and at an ice-glass interface [12]. Finally, measurements of *wire regelation* (the motion of wires through ice) at low temperatures have provided indirect evidence of a fluid film at the ice-wire interface [13(a)].

Since we are not focusing on solid-vapor or solid-solid interfaces we note evidence for premelting in these systems only in passing. In the former case, metals and rare gases exhibit surface melting [8] and liquid layers have been observed at the free ice surface [15] and are consistent with *incomplete* surface melting, wherein the liquid attains a finite thickness at the bulk transition. In the case of grain boundaries, lattice-gas models have

predicted disordered phases [16], where, well below the bulk melting point T_m, there is a gradual but clearly defined transition in the structure and thermodynamic properties of the boundary. Similar models of a tilt grain boundary find that the interface is unstable to the intrusion of a solid of an intermediate orientation [17], and molecular dynamics calculations of Lennard-Jones solids [18] exhibit an orientation dependence of grain boundary disorder.

B. Dynamics

In this paper we explore the dynamical effects associated with thermolecular pressure *gradients* acting on premelted films. Both microscopic and macroscopic theory for the spreading of liquids on solids have a rich literature [19]. Particularly relevant to our study is the spreading of a wetting layer under the influence of a gradient in the disjoining pressure [19]. For a liquid-vapor system, the nongradient case of wetting inside a capillary has been treated [20], and has a correspondence to the problem of wetting on a cylindrical fiber [19(c)]. Although dynamical studies concerning premelted films are rare, the relation between thermomolecular pressure in unfrozen water and frost-heave phenomena has been discussed from several perspectives [11,21,22]. Other ice studies include one under isothermal conditions [23], which required the introduction of an anisotropic pressure tensor through the film, and a continuum model for frost heave in an ice-water-particle mixture requiring parametrization of bulk hydraulic permeabilities [13(b)]. The latter study contains many of the essential physical ingredients of the heave mechanism.

In what follows we consider only unretarded van der Waals interactions, and explore the dynamical consequences of imposing a temperature gradient on a confined premelted film. For the analysis proper we digress from the commonly studied planar situation and examine behavior in an idealized geometry, viz., a single cylindrical pore or capillary. The capillary is at a temperature below the bulk melting transition of the material, and a thin film separates the solid from the capillary walls (Fig. 1). On imposition of an axial temperature gradient, gradients in the film thickness and thermomolecular pressure develop. This allows us to investigate relatively unexplored dynamics in a simple geometry. Moreover, by studying a confined film, we avoid potential problems associated with a free surface [7]. A primary motivation of our study is to form a theoretical framework within which the experiments of Wilen and Dash [21] can be interpreted.

In the next section we review the physics of interfacial premelting and thermomolecular pressure. We then develop a simple model of solidification in a capillary tube that includes effects of interfacial premelting, and solve two, experimentally achievable, initial value problems. For the case of a transient thermal field, we solve the equations approximately by the method of matched asymptotics and check the results numerically. We then solve the case of a steady thermal field and find a marked change in the deformation behavior. We conclude with

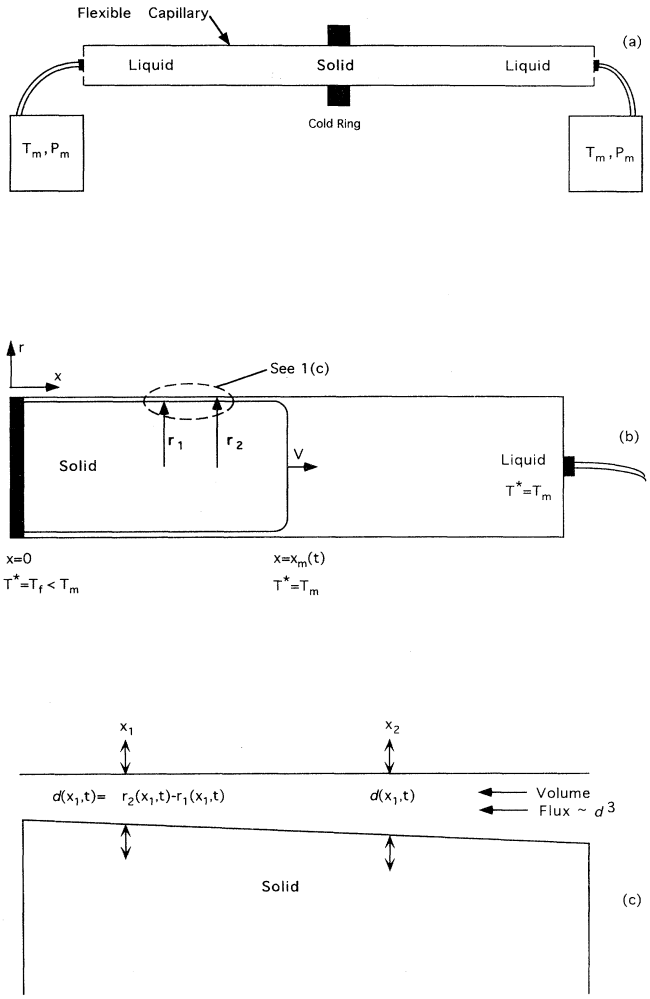

FIG. 1. A schematic of the capillary gedanken experiment, which is patterned after the experiments of Wilen and Dash [21]. In (a) we display a cross section of the entire system which consists of a flexible capillary tube filled with the material of interest centered on a cold ring. The walls of the tube (with the exception of the small region adjacent to the ring) are insulated so that only axial heat currents are allowed. Initially we envisage the system to consist of solid and liquid in coexistence at $T^* = T_m$ so that we must have $T_f = T_m$. The liquid region is allowed to communicate with a reservoir which has independent temperature and pressure control. The length of the capillary is orders of magnitude greater than its diameter. (b) We take the cold ring to be a plane of symmetry and begin an experiment by quenching it to $T_f < T_m$. This establishes a temperature gradient across the solid which drives it into the isothermal melt. The radius of the solid finger is r_1 and that of the tube is r_2. At a given temperature the interfacially melted film has thickness $r_2 - r_1 = d = \lambda t_r^{-1/3}$. The position of the moving "bulk" interface $x_m(t)$ is unknown in the problem. (c) The imposed temperature gradient establishes a thermomolecular pressure gradient (see text) which drives a lubrication flow in the region between the solid and the membrane with a volume flux $Q \propto d^3$. Material in excess of the thickness given by $d = \lambda t_r^{-1/3}$ solidifies and the membrane is distorted in a manner to be determined.

a discussion of the results, their experimental basis, and their various applications.

II. PREMELTING AND THERMOMOLECULAR PRESSURE

The focus here is on the interface between a solid and a nonreactive, uncorrugated substrate. When asking whether or not a layer of melt intervenes between the solid and the substrate several approaches to the problem have proved useful. One approach uses the full frequency dependent theory of dispersion forces to find the thickness d of the layer that minimizes the excess free energy at a fixed temperature [14]. In such an approach, the γ's are the interfacial free energies per unit area of the solid-wall (sw), solid-liquid ($s\ell$), and liquid-wall (ℓw) boundaries, with implicit reference to the crystallographic orientations present at an interface. The excess free energy is then written as $\gamma_{s\ell} + \gamma_{\ell w} + F(d)$, where $F(d)$ is the frequency dependent excess free energy associated with the layer. Complete interfacial melting is indicated by a divergence of d as the free energy minimum is approached where $\gamma_{sw} = \gamma_{s\ell} + \gamma_{\ell w}$. Another approach is based on the notion that, if the interface is wetted by the liquid phase, at temperatures below the bulk melting point T_m then the free energy of the wet system is lower than that of the dry system [3,8,11]. Thus, if the interface were initially dry at small reduced temperature $t_r = (T_m - T^*)/T_m$ (T^* is the actual temperature), the system's free energy could be lowered by converting a layer of solid to liquid. One deposits a layer of thickness d and then minimizes the system's mean-field free energy: equilibrium comes as a balance between interfacial energies, which act to decrease the total free energy with increasing d, and bulk free energies which assess a penalty for the maintenance of a supercooled liquid. For thin films at small t_r, the penalty is not prohibitive, and the film persists. Complete interfacial melting is indicated by a divergence of d as T_m is approached from below. The form of the divergence (e.g., power law or logarithmic) depends on the basic interactions in the materials. While these and other approaches differ in detail (e.g., interparticle interaction potentials), they all agree that on surfaces of many solids thin liquid films are thermodynamically stable below their bulk melting temperatures.

To study the dynamics of these films, we take a modified view of the second approach above. If the solid-wall interface is wetted by a macroscopic layer of the melt ($\mathcal{M}$) of thickness d at temperature T^*, the mean-field free energy of the system is composed of bulk and surface terms. The total grand potential is

$$\Omega = -P_{\mathcal{M}} V_{\mathcal{M}} - P_s V_s + \mathcal{I}(d), \tag{1}$$

where P and V denote pressure and volume, and the interfacial term $\mathcal{I}(d)$ captures the free energy benefit (decrease) of increasing the film thickness. We write $\mathcal{I}(d) = [\Delta\gamma f(d) + \tilde{\gamma}_{sw}] A_{s\mathcal{M}}$, where $\Delta\gamma = \gamma_{s\ell} + \gamma_{\ell w} - \tilde{\gamma}_{sw}$, and $\tilde{\gamma}_{sw}$ is the nonequilibrium measured value of the solid-wall interfacial free energy (see Appendix and Ref. [1]). At $t_r > 0$, there is an effective interaction between the two interfaces, which will depend on their separation. The function $f(d)$ represents the algebraic decay due to van der Waals interactions between a film of thickness d and the two other materials which it separates: $f(d) = 1 - (\frac{d}{\sigma})^{-\alpha+1}$, where σ is on the order of a molecular diameter and $\alpha = 3$ for nonretarded and $\alpha = 4$ for retarded dispersion forces. Thus, $\mathcal{I}(d)$ displays the asymptotic behavior of the thickness dependent excess Helmholtz free energy per unit area from the full frequency dependent dispersion theory in the case where complete surface melting occurs [14,24]. In complete interfacial melting the dry interface is more costly than the wet interface, so $\Delta\gamma < 0$. The minimum of Ω occurs at fixed temperature and chemical potential, $\mu_{\mathcal{M}}(T^*, P_{\mathcal{M}}) = \mu_s(T^*, P_s) \equiv \mu$, thus for fixed total volume the minimization with respect to d occurs when the pressure difference between the melt layer and the solid is

$$P_{\mathcal{M}} - P_s = \Delta\gamma(\alpha - 1)\left(\frac{1}{\sigma}\right)^{-\alpha+1} d^{-\alpha}. \tag{2}$$

Hence, the pressure is uniform in each phase, but the interfacial term is responsible for a pressure difference between the melted layer and the bulk solid, which is known in the context of wetting as the *disjoining pressure* [19]. The pressure in the melted layer cannot be directly measured in equilibrium. Rather, the difference expressed in Eq. (2) represents the tendency for the interfaces to repel; an effect realized dynamically.

The essential qualitative features of frost heave can be realized directly from Eq. (2), which becomes $P_{\mathcal{M}} = P_s + 2\Delta\gamma\sigma^2 d^{-3}$ for nonretarded interactions. We imagine maintaining P_s at some fixed value. By assumption, the film thickness increases with temperature, so that the pressure in the film, $P_{\mathcal{M}}$, must also increase with temperature. Hence, on imposition of a temperature gradient parallel to the interface, premelted liquid will be driven along the interface from high to low temperature where it eventually freezes. Complete interfacial melting occurs at $T^* = T_m$, and the film thickness diverges, so that $P_{\mathcal{M}} = P_s = P_m$, where P_m is the pressure in a reservior which is in contact with the layer. To study the detailed dynamics of interfacially melted films, we must derive a number of additional thermodynamic results.

We are interested in the region of the phase diagram where the solid is the stable *bulk* phase. Expanding the chemical potential of a region j about (T_m, P_m) to first order [25] and using the Gibbs-Duhem relationship yields

$$\mu_j(T^*, P_j) = \mu_j(T_m, P_m) - s_j(T^* - T_m) + \frac{(P_j - P_m)}{\rho_j}, \tag{3}$$

where s_j is the entropy per unit mass. The intensivity of chemical potential requires that in thermodynamic equilibrium the chemical potential of the melted layer is equal to that of the solid,

$$\mu_s(T^*, P_s) - \mu_{\mathcal{M}}(T^*, P_{\mathcal{M}})$$

$$= -q_m t_r + \frac{(P_s - P_m)}{\rho_s} - \frac{(P_{\mathcal{M}} - P_m)}{\rho_{\mathcal{M}}} = 0, \quad (4)$$

where q_m is the latent heat of fusion per molecule. As has been pointed out previously [11], on considering the density of the melted region to be equivalent to the bulk liquid density ($\rho_{\mathcal{M}} = \rho_\ell$), one can express the pressure difference $P_{\mathcal{M}} - P_s$ as a universal thermodynamic function, independent of the interaction potential. Rewriting Eq. (4) we obtain

$$P_{\mathcal{M}} - P_s = -\rho_\ell q_m t_r - (1 - \rho_\ell/\rho_s)(P_s - P_m). \quad (5)$$

When the pressure in the liquid layer is constant, equal to the reservoir pressure P_m, a dynamic equilibrium is established and Eq. (5) provides

$$P_s - P_m = \rho_s q_m t_r. \quad (6)$$

Thus, in equilibrium, the pressure builds up to a value proportional to t_r. For example, this pressure in water is 11 atm $^\circ C^{-1}$ and in Ar 5.7 atm $^\circ C^{-1}$, and values for other materials have been tabulated elsewhere [3,11]. In porous media, this is referred to as the *maximum frost-heave pressure*, which is the maximum pressure that can build up as a result of the flow of unfrozen liquid to the freezing front [11]. When P_s reaches this value, opposed by an equal *overburden pressure* from the wall, the flow ceases. When the wall exerts no overburden pressure, fluid flows from the reservoir through the thin film, and towards the solid-liquid interface, where it solidifies to heave or distort the wall. Note that, in the case of water, it is *not* the pressure associated with volumetric expansion during the phase change that creates the frost-heave pressure, as this could be taken up by the reservoir.

Combining Eqs. (2), (5), and (6) yields an expression for the temperature dependence of d that depends on the nature of the intermolecular forces. For unretarded ($\alpha = 3$) van der Waals forces, the dependence is a well known power law [2,8] in the reduced temperature:

$$d = \left(-2\sigma^2 \frac{\Delta\gamma}{\rho_s q_m}\right)^{1/3} t_r{}^{-1/3} \equiv \lambda t_r{}^{-1/3}. \quad (7)$$

For thin metal films, where charge fluctuations are screened by the film conductivity, the resulting short range potential leads to an exponential behavior $\partial f/\partial d \propto \exp(-cd)$, where c is a constant. This provides logarithmic temperature dependence, $d \propto |\ln t_r|$ [8]. Other types of interactions lead to similarly specific temperature dependences. To provide some intuition we note that Gilpin's data [13(a)] for ice against various metals are consistent with a film thickness of about 35 Å at $T^* = -1\,^\circ C$, and Wilen and Dash's data [21] for ice against a plastic are consistent with films this thick when $T^* > -0.025\,^\circ C$.

When the solid is in equilibrium with the reservoir, one can determine the pressure gradient that drives the flow in the liquid layer by setting $P_s = P_m$:

$$P_{\mathcal{M}} - P_m = -\rho_\ell q_m t_r. \quad (8)$$

Since the pressure decreases for decreasing temperature, fluid flows towards lower temperatures. The pressure difference or *thermomolecular pressure* given by Eq. (8) is negative and can be viewed as a shift of the chemical potential of the film from the reference state defined by the reservoir [3,11]. Hence transport of liquid realized by imposing a temperature gradient reflects the gradient in chemical potential.

Studying the case in which there is flow in a confined premelted film requires that the overburden pressure is greater than P_m, but less than the maximum frost-heave pressure given by Eq. (6). This general condition follows from Eq. (4):

$$P_{\mathcal{M}} - P_m = -\rho_\ell q_m t_r + \frac{\rho_\ell}{\rho_s}(P_s - P_m). \quad (9)$$

Thus, as stated above, a temperature gradient along the interface creates a *thermomolecular pressure gradient* [11] which drives flow in the premelted film. This is analogous to a gradient in the disjoining pressure along a wetting substrate [19]. Next we describe our study of the dynamics of this film in a confined geometry.

III. SOLIDIFICATION IN A CAPILLARY TUBE

The thickness of an interfacially premelted layer is uniform in isothermal systems. Hence direct experimental searches for premelting have focused on probing isothermal systems for liquid fraction. Here, we are motivated by the experiments of Wilen and Dash [21] on pure H_2O ice, in which a temperature gradient is imposed parallel to the premelted interface and the subsequent dynamics is probed by interference microscopy. This novel approach has the advantage of exposing the essential physics of the problem in the absence of impurity and curvature effects [9], which complicate the analysis. Their apparatus is geometrically more complicated than that we consider here, and an explicit comparison is the subject of a future presentation. We consider a flexible capillary tube that is insulated around its diameter (with the exception of the small region in the center), but can conduct heat axially (Fig. 1). The tube is centered on a cold ring and filled with a pure liquid. Note that we eventually study H_2O ice, but our analysis is general and requires only that the material in question interfacially premelts in the mean-field sense outlined above. If the system is maintained at a uniform undercooling t_r, then the capillary is filled with the solid phase surrounded by a thin annular film of thickness given by Eq. (7). The film is in contact with a bulk reservoir at T_m, P_m so there is an infinite supply of the liquid phase available to the annular region.

Consider an initial state that is liquid and isothermal at temperature T_m. An experiment begins by cooling the middle of the cold ring to a value $T_f < T_m$ so that the vertical solid-liquid interface at $x_m(t)$ grows axially along the capillary (Fig. 1). The approach to local phase equi-

librium is assumed to be very rapid relative to changes in the temperature, so at each position $0 < x < x_m$ the temperature $T^*(x,t)$ determines the film thickness $d(x,t) = r_2(x,t) - r_1(x,t)$ according to Eq. (7). The temperature gradient is responsible for an axisymmetric thermomolecular pressure gradient which, according to Eq. (9), is given by

$$\partial_x P_\ell = \frac{\rho_\ell q_m}{T_m}\partial_x T^* + \frac{\rho_\ell}{\rho_s}\partial_x P_s. \tag{10}$$

Note we have written $P_{\mathcal{M}} = P_\ell$ since we are treating the film as bulk liquid. This pressure gradient drives a lubrication flow in the thin film $U(r)$ given approximately by

$$U(r) = \frac{-\partial_x P_\ell}{2\eta}(r - r_1)(r_2 - r), \tag{11}$$

in the limit $d \ll r_1$ [26], where η is the dynamic viscosity of the bulk liquid. The mass flux Q_m is given by

$$Q_m = \int_{r_1}^{r_2} dr \rho_\ell 2\pi r U(r) = -\frac{\pi}{6}\frac{\rho_\ell \partial_x P_\ell}{\eta} r_2 d^3. \tag{12}$$

Hence there is flow along the thin film, and liquid material in excess of the equilibrium thickness [Eq. (7)] at a given local undercooling must solidify, increase the radius of the solid, and thereby increase the capillary radius $r_2(x)$. Mass conservation requires that

$$\partial_t(\pi {r_2}^2) + \partial_x Q = 0, \tag{13}$$

where t denotes time and Q is the volume flux, which we now write explicitly using Eq. (10) as

$$Q = \frac{r_2 d^3}{6\eta}\left(\frac{\rho_\ell}{\rho_s}\partial_x P_s - \rho_\ell q_m \partial_t t_r\right). \tag{14}$$

The pressure at each point x in the solid is opposed by the restoring force of the capillary membrane. For simplicity, we assume that the capillary walls only exert a hoop stress, which is a good approximation if the deformation varies slowly with axial distance. In addition, we assume linear elasticity,

$$P_s = k(r_2 - r_0),$$

where k is a constant, and r_0 is the undeformed radius of the capillary tube. Equations (13) and (14) can be combined to yield an equation for the capillary radius r_2,

$$\partial_t r_2 - \frac{\rho_\ell \pi k \lambda^3}{12\eta\rho_s}\partial_x\left[\frac{T_m}{T_m - T^*}\partial_x\left\{r_2 - r_0 - \frac{\rho_s q_m}{\pi k T_m}(T_m - T^*)\right\}\right] = 0, \tag{15}$$

which depends solely on the temperature T^*.

On cooling the cold ring, a temperature gradient is established across the solid. Since the melt region is held at T_m, any gradient causes the bulk solid to grow at the expense of the liquid. Thus we have a type of Stefan problem [27] which is coupled to the mass transport through the thin film via Eq. (15). Heat is conducted along the solid and latent heat is released as liquid in the thin film solidifies. Hence conservation of thermal energy gives

$$\partial_t T^* = \kappa \partial^2{}_{xx} T^* + \frac{2q_m}{c_p r_0}\partial_t r_2, \tag{16}$$

where c_p and κ are the specific heat at constant pressure and the thermal diffusivity of the solid. We use these values because, in the region $0 < x < x_m$, the volume fraction is dominated by the solid and so it will carry almost all of the heat.

The governing equations given above form a system of coupled, partial differential equations, which require the following boundary and auxiliary conditions. At the cold ring $x = 0$ we have

$$T^* = T_f \qquad (x = 0), \tag{17}$$

where T_f is an experimental control. With regard to the thin film flow, $x = 0$ is a symmetry plane at which the liquid volume flux Q must vanish, and so from Eq. (15) we have that

$$\partial_x(r_2 - r_0) = \frac{\rho_s q_m}{\pi k T_m}\partial_x(T_m - T^*) \qquad (x = 0). \tag{18}$$

At time t the bulk solid-liquid interface is located at $x = x_m(t)$ where the temperature is given by

$$T^* = T_m \qquad [x = x_m(t)]. \tag{19}$$

Since there is no ice within the dispersion force range of the membrane, there is no deformation there, which gives

$$r_2 - r_0 = 0 \qquad [x = x_m(t)]. \tag{20}$$

The position of the interface is determined by solving the field equations and boundary conditions subject to the usual Stefan condition expressing conservation of heat,

$$\kappa \partial_x T^* = \frac{q_m}{c_p}\partial_t x_m \qquad [x = x_m(t)]. \tag{21}$$

Finally, at $x = x_m(t)$, condition (19), on the temperature at the bulk phase boundary, introduces a singularity in Eq. (15), which implies an infinite volume flux in the film unless

$$\partial_x(r_2 - r_0) = \frac{\rho_s q_m}{\pi k T_m}\partial_x(T_m - T^*) \qquad [x = x_m(t)]. \tag{22}$$

This is not an imposed boundary condition but has been determined as a necessary condition on the solution of the equations.

We are chiefly concerned with the nonretarded regime, but we note several phenomena that are of interest as $x \to x_m$ (Fig. 1). First, as x increases, one will encounter a point, say x_{nr}, where retardation may control the film thickness, and the retarded power law will be-

come relevant. Second, as x increases further, Gibbs-Thomson effects will influence the phase boundary geometry; the solid-liquid interface is out of the dispersion force range of the membrane. Finally, the lubrication approximation will break down in the same subdomain, $\delta x = (x_m - x_{nr})/x_m \ll 1$. We will find that these effects do not alter the essential features of our analysis, but we will pursue some of their implications in future publications.

IV. SIMILARITY SOLUTION: TRANSIENT THERMAL FIELD

We first consider the capillary to be infinite in the x direction, so since there is no externally imposed time scale Eqs. (15) and (16) and the associated boundary and auxiliary conditions admit a similarity solution. The scalings for the capillary displacement and temperature are chosen as follows. Balancing the second and third terms of Eq. (15) suggests $r_2 - r_0$ scales with $\rho_s q_m \Delta T/\pi k T_m$, where $\Delta T = T_m - T_f$ is an appropriate scale for temperature differences in the system. The time evolution of the system is diffusive in character, which leads to the similarity variable $\xi = x/2\sqrt{\kappa t}$. The similarity solution of our dimensionless field equations depends solely on ξ and can be written as

$$r_2 - r_0 = \beta R(\xi)$$

and

$$T_m - T^* = \Delta T\, T(\xi), \tag{23}$$

where $\Delta T = T_m - T_f$ and $\beta = \rho_s q_m \Delta T/\pi k T_m$ is a length scale characteristic of the deformation of the wall. It is the product of the *thermomolecular pressure coefficient* $\rho_s q_m/T_m$, which is solely due to the properties of the material, and an experimental parameter which is the ratio of the thermal drive for the thermomolecular pressure ΔT and the strength of the capillary k.

With these scalings Eqs. (15) and (16) can be written in dimensionless form as follows:

$$-2\xi R' = \epsilon \left[\frac{1}{T}(R' - T')\right]', \tag{24}$$

$$-2\xi T' = T'' + 2\mathcal{S}\xi \mathcal{R}', \tag{25}$$

where the primes denote differentiation with respect to ξ. The dimensionless parameters are $\epsilon = \rho_\ell \pi k \Lambda T_m/12\kappa\eta\rho_s\Delta T$, with $\Lambda = \lambda^3$ as defined by Eq. (7), and $\mathcal{S} = 2q_m\beta/c_p\Delta T r_0 \equiv 2S\beta/r_0$, with $S = q_m/c_p\Delta T$ being the usual Stefan number. The symmetry plane and the "bulk" phase boundary are located at $\xi = 0$ and $\xi = \xi_m$, respectively, so that boundary conditions (17)–(21) become

$$T = 1 \qquad (\xi = 0), \tag{26}$$

$$R' = T' \qquad (\xi = 0), \tag{27}$$

$$T = R = 0 \qquad (\xi = \xi_m), \tag{28}$$

and

$$T' = -2S\xi_m \qquad (\xi = \xi_m), \tag{29}$$

where Eq. (29) is the Stefan condition. The singularity in Eq. (24) when $T = 0$ (at $\xi = \xi_m$) necessitates the condition

$$R' = T' \qquad (\xi = \xi_m). \tag{30}$$

We estimate an appropriate magnitude for the dimensionless parameter $\epsilon = \rho_\ell \pi k \Lambda T_m/12\kappa\eta\rho_s\Delta T$ as follows. We focus on the ice-water system and use $\rho_\ell/\rho_s = 1.091$, $T_m = 273.16$ K, $\kappa = 1.2 \times 10^{-6}$ m^2 s^{-1}, $\eta = 1.37 \times 10^{-3}$ kg/m s, and $\Lambda = 1.57 \times 10^{-28}$ m^3, the latter determined from a fit of Gilpin's data [13(a)] in the temperature range $-0.01 < T^* < -10\,^\circ$C using the van der Waals exponent [8(c)]. An experimenter has some freedom to choose ΔT and k. The temperature scale ΔT will typically be in the range 1–10 K. The value of k is determined by the material forming the capillary tube and the thickness of its walls, and should be chosen small enough to allow measurement of the wall displacement. If the diameter of the tube is 1 mm, say, then a 10% displacement (i.e., 100 μm) is easily detectable using optical techniques. The maximum displacement is that which gives the maximum frost-heave pressure $P_m + \rho_s q_m t_r = \pi k(r_2 - r_0)$. Therefore, for flow to persist throughout the domain $0 < x < x_m$, k should be chosen to be less than about 3×10^{11} Pa m^{-1}. This value of k gives an upper bound to ϵ of about 10^{-4}. Since $\epsilon \ll 1$, we seek an asymptotic solution of the equations as follows.

Solution by matched asymptotic expansions

1. The outer solution

We proceed by seeking solutions to the leading-order equations obtained by setting $\epsilon = 0$ in Eqs. (24) and (25). This gives

$$T_0'' = -2\xi T_0', \tag{31}$$

$$R_0' = 0. \tag{32}$$

Equation (31) satisfies all the thermal boundary conditions (26), (28), and (29). The solution is simply that of the classical Stefan problem, namely,

$$T_0 = 1 - \frac{\mathrm{erf}\xi}{\mathrm{erf}\xi_m}, \tag{33}$$

with

$$\sqrt{\pi}\xi_m e^{\xi_m^2}\mathrm{erf}\xi_m = S^{-1} \tag{34}$$

[27]. Equation (31) has the solution

$$R_0 = \bar{R}_0 \quad (\text{const}), \tag{35}$$

which satisfies neither the boundary condition (27) nor

the singularity condition (30). The perturbation $\epsilon \to 0$ is a singular perturbation of Eq. (24). Physically, the leading-order solution does not capture behavior in regions where the gradients are large. To proceed, we require boundary layers at both ends of the domain, and we shall ultimately determine $\bar{R}_0$ by matching with the boundary-layer solutions [28].

2. Boundary layer near $\xi = 0$

In this region we require that $R' \sim T' = O(1)$ and that both sides of Eq. (24) balance, which suggests introducing the rescaling

$$\eta = \epsilon^{-1/2}\xi, \qquad R = \epsilon^{1/2}F(\eta). \tag{36}$$

Proceeding as in the outer region, the leading-order equation for the boundary layer becomes

$$-2\eta F_0' = F_0'', \tag{37}$$

which is subject to the boundary and matching conditions

$$F_0' = -\frac{2}{\sqrt{\pi}\,\mathrm{erf}\xi_m} \qquad (\eta = 0), \tag{38}$$

$$F_0 \to \epsilon^{-1/2}\bar{R}_0 \qquad (\eta \to \infty). \tag{39}$$

The leading-order inner solution is thus

$$F_0 \sim \epsilon^{-1/2}\bar{R}_o + \frac{\mathrm{erfc}\eta}{\mathrm{erf}\xi_m}. \tag{40}$$

Since $F_0 = O(1)$, Eq. (40) or, equivalently, the matching condition (39), shows that $\bar{R}_0 = O(\epsilon^{1/2})$.

3. Boundary layer near $\xi = \xi_m$

In this region we seek the same balances as previously, namely, that $R' \sim T'$ and that the two sides of Eq. (24) must balance. However, since T is also small in this region it must be rescaled along with R and ξ. We are led to the following scaled variables:

$$\zeta = \epsilon^{-1/2}\sqrt{2S}\,\xi_m(\xi_m - \xi), \qquad R = \epsilon^{1/2}\sqrt{2S}\,G(\zeta),$$
$$T = \epsilon^{1/2}\sqrt{2S}\,H(\zeta). \tag{41}$$

The leading-order equations in this boundary layer are then

$$G_0'' - \frac{1}{\zeta}G_0' - 2\zeta G_0' + \frac{1}{\zeta} = 0, \tag{42}$$

$$H_0'' = 0 \tag{43}$$

which are subject to the boundary conditions

$$G_0 = H_0 = 0, \quad H_0' = G_0' = 1 \qquad (\zeta = 0), \tag{44}$$

$$G_0' \to 0 \qquad (\zeta \to \infty). \tag{45}$$

The solution of Eq. (42) is

$$G_0 = \frac{\sqrt{\pi}}{2}\left(1 - e^{\zeta^2}\mathrm{erfc}\zeta\right), \tag{46}$$

where we have used the solution to Eq. (43) to show that, in this boundary layer, $H_0 = \zeta$, i.e., that the temperature is appoximately linear. From Eq. (46), we see that

$$G_0 \sim \frac{\sqrt{\pi}}{2} + O(\zeta^{-2}) \quad \text{as} \quad \zeta \to \infty, \tag{47}$$

which shows that the constant inferred from Eq. (35) has the value

$$\bar{R}_0 = \sqrt{\frac{\epsilon S\pi}{2}}. \tag{48}$$

4. A composite solution

At this stage we can form a uniformly valid asymptotic solution [28]

$$R_C = R_0 + F_0 + G_0 - \lim_{\eta\to\infty} F_0 - \lim_{\zeta\to\infty} G_0, \tag{49}$$

which gives

$$R_C = \epsilon^{1/2}\left\{\frac{\mathrm{erfc}\left(\frac{\xi}{\sqrt{\epsilon}}\right)}{\mathrm{erf}\xi_m} + \sqrt{\frac{\pi S}{2}}\left[1 - \exp\left(\frac{2S}{\epsilon}\xi_m^2(\xi_m - \xi)^2\right)\right.\right.$$
$$\left.\left.\times\mathrm{erfc}\left(\sqrt{\frac{2S}{\epsilon}}\xi_m(\xi_m - \xi)\right)\right]\right\}, \tag{50}$$

where ξ_m is determined as the root of Eq. (34). The first and third terms are the boundary layers near $\xi = 0$ and ξ_m, and the second (constant) term represents the "outer" solution which is the middle region in Fig. 2 where the deformation is uniform. This solution, shown in Fig. 2(b), is *universal* in that it has the same form for all values of dimensional time and space [within the domain $0 < x < x_m(t)$].

A comparison between the composite solution and a numerical solution of the full similarity equations is shown in Fig. 2(a) for a value of $\epsilon = 0.1$. The agreement is very good, and it will be even better for smaller values of ϵ. Thus the composite expansion provides an excellent approximation for practical use.

In Fig. 2(c), we show the composite solution for $\epsilon = 10^{-4}$, plotted as a function of distance for various times. This figure is representative of what would be seen in a typical experiment. Note that a finger of ice appears to push into the capillary, forcing it open at the nose. Of course, the ice is not being pushed, and the actual mechanism of heave is as follows. During the time scale of deformation the temperature gradient is approximately uniform along the tube, which implies that the thermomolecular pressure gradient is almost uniform. However, the premelted film is thickest near the nose, where the undercooling is lowest, and decays over a short distance

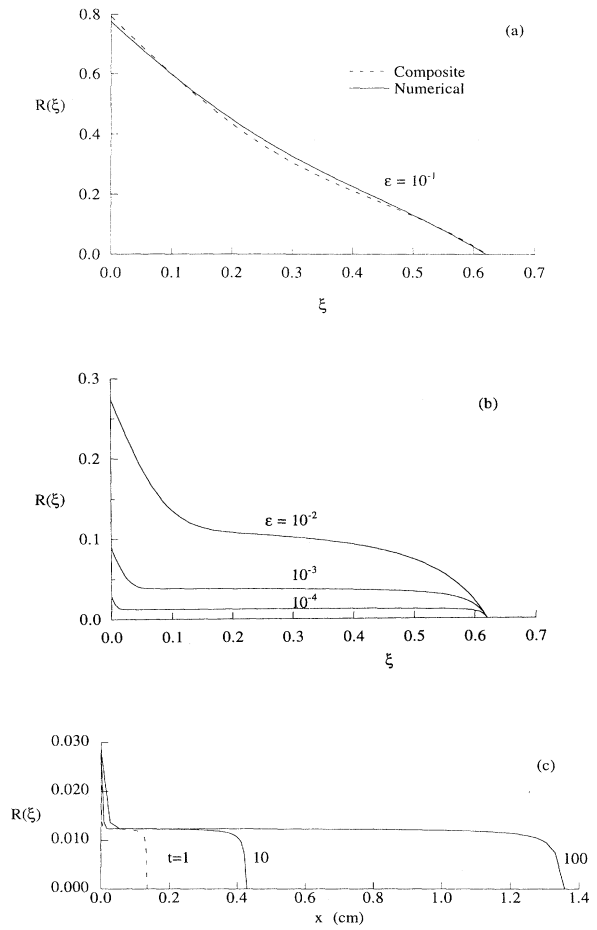

FIG. 2. (a) A comparison between the composite solution of dimensionless (*universal*) similarity solution for wall displacement R as a function of the dimensionless similarity variable ξ, with a transient thermal field, Eq. (50), and a numerical solution for $\epsilon = 0.1$. The material is pure H_2O ice, and the thermal properties are commonly available. (b) The composite solution for R as a function of ξ for three values of the parameter ϵ. Note that, when ϵ is small, the wall displacement is almost uniform along the capillary, and that by the scaling of the deformation [Eq. (23)], R increases with ϵ. (c) The composite solution for $\epsilon = 10^{-4}$ as a function of position at t =1, 10, and 100 min.

$\delta = O(\epsilon^{1/2})$ towards the cold ring. Hence there is a large flow of water in the film near the nose, which freezes to cause heave. Away from the nose, due to the smallness of the van der Waals coefficient λ, the film flow is weak and there is little further heave. Thus the displacement of the capillary wall is approximately uniform away from the nose. The volume flux that drives the deformation decreases at a rate that scales with the rate of motion of the bulk interface ($\propto t^{-1/2}$). Hence the deformed region of the capillary maintains the same shape as the solid finger grows down the tube. The larger displacement near the center of the capillary is a remnant from the initial moments when the temperature gradient and, hence, the thermomolecular pressure gradient were large everywhere.

It is important to note that the displacement $R = O(\epsilon^{1/2}) \ll 1$ during the transient phase of an experiment, which is described by the similarity solution presented in this section. In a finite-sized experiment, the ice can stop advancing and the temperature field can become steady, but capillary flow will continue until the displacement of the wall provides sufficient elastic pressure to counteract the thermomolecular pressure. We analyze this situation in the next section.

V. SIMILARITY SOLUTION: CONSTANT TEMPERATURE GRADIENT

We now analyze the capillary deformation for a case in which the temperature gradient is held at a constant value $\mathcal{G}$. We choose coordinates such that the bulk solid-liquid interface is located at the fixed position $x = 0$ and x increases towards the cold ring. This allows a simple representation of the temperature field as $T^*(x) = T_m - \mathcal{G}x$, and Eq. (15) for mass conservation becomes

$$\partial_t r_2 - \frac{\rho_\ell \pi k \Lambda T_m}{12\eta\rho_s \mathcal{G}} \partial_x \left[\frac{1}{x} \partial_x \left(r_2 - r_0 - \frac{\rho_s q_m}{\pi k T_m} \frac{\mathcal{G}}{x} \right) \right] = 0. \tag{51}$$

This equation also admits a similarity solution but with a different variable $\varsigma = x/\delta$, where

$$\delta = \left(\frac{\pi k \Lambda T_m}{12\rho_s \nu \mathcal{G}} \right)^{1/3} t^{1/3}. \tag{52}$$

The similarity solution for capillary deformation is given by

$$r_2 - r_0 = \mathcal{H} g(\varsigma) \quad \text{with} \quad \mathcal{H} = \frac{\rho_s q_m \mathcal{G}}{\pi k T_m} \delta. \tag{53}$$

The length scale $\mathcal{H}$ is time dependent and expresses the effect of the driving force and the capillary strength on the deformation at a given time.

The dimensionless, ordinary differential equation for the capillary deformation, derived from Eq. (51), is

$$g - \varsigma g' = 3 \left[\frac{1}{\varsigma} (g' - 1) \right]', \tag{54}$$

where the primes denote differentiation with respect to ς. Solutions to Eq. (54) are required to satisfy the boundary and auxiliary conditions

$$g = 0 \qquad \text{and} \qquad g' = 1 \qquad (\varsigma = 0), \tag{55}$$

and

$$g \to 0 \qquad (\varsigma \to \infty). \tag{56}$$

Equation (54) was solved using a numerical shooting method in which the curvature g'' at $\varsigma = 0$ was varied until the boundary condition (56) was satisfied. The (*universal*) similarity solution is plotted in Fig. 3(a), and the

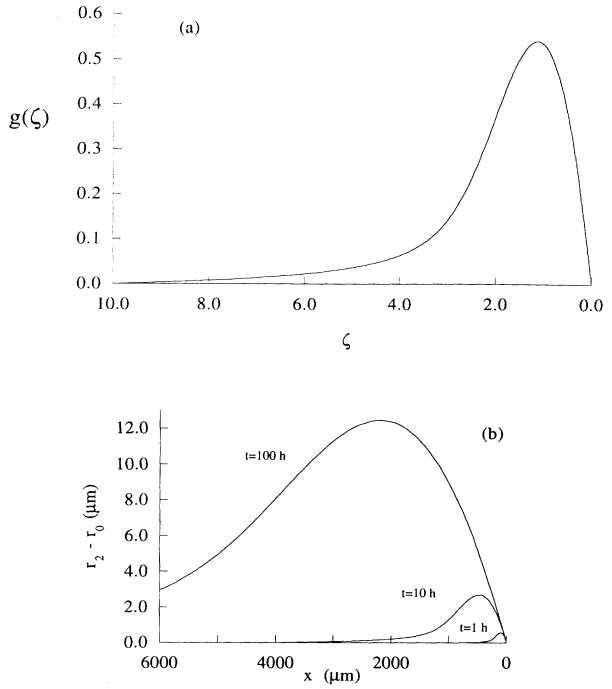

FIG. 3. (a) Plot of the dimensionless (*universal*) similarity solution for the deformation g as a function of ς when the temperature gradient is fixed. The material is pure H_2O ice. Note the marked contrast with the solution of the transient problem. (b) The dimensional deformation as a function of position at t =1, 10, and 100 h. Here, we have chosen $\mathcal{G}$=1 K m^{-1} and k=3×10^9 Pa m^{-1}.

dimensional deformation as a function of position from the bulk solid-liquid interface is plotted in Fig. 3(b). The maximum deformation $g_{max} \approx 0.541$ occurs at position $\varsigma_{max} \approx 1.14$.

Since the temperature field is steady, the gradient in the volume flux is constant, and thermocapillary flow in the thin premelted liquid film causes further evolution of the system. The liquid is drawn into the film by the thermomolecular pressure and freezes, causing the capillary tube to deform. The position of maximum deformation moves towards the colder end of the tube; its position is given by

$$x_{max} \approx 1.14 \left(\frac{\pi k \Lambda T_m}{12 \rho_s \nu \mathcal{G}} \right)^{1/3} t^{1/3}. \quad (57)$$

The maximum displacement increases with time according to

$$(r_2 - r_0)_{max} \approx 0.541 \left(\frac{\Lambda}{12\nu} \right)^{1/3} \left(\frac{\rho_s \mathcal{G}}{\pi k T_m} \right)^{2/3} t^{1/3}. \quad (58)$$

The principal experimental controls are the temperature gradient $\mathcal{G}$ and the elastic strength of the capillary k. We see from the expressions above, and Fig. 4, that large deformations can be achieved by choosing $\mathcal{G}$ large

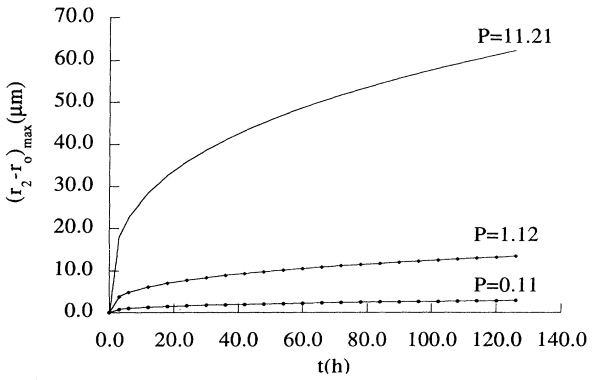

FIG. 4. Plot of the maximum displacement as a function of time for various values of the dimensionless parameter $P = 3\mathcal{G}\rho_s q_m / k T_m$, in which $\rho_s q_m / T_m$ is the frost-heave pressure 1.121×10^6 Pa m^{-1} = 11 atm °C^{-1}, and we use the former units here. The material is pure H_2O ice.

and k small, while the temporal migration of the peak deformation will be most apparent when $\mathcal{G}$ is small and k large. Note also that the width of the peak scales in the same way as x_{max}, so will be broader for small values of $\mathcal{G}/k$, and will narrow and shift toward the bulk solid-liquid interface as $\mathcal{G}/k$ increases.

The qualitative features of this solution, with a local maximum in the deformation near the bulk interface, are in agreement with the experimental findings of Wilen and Dash [21]. In their experiments, the temperature gradient is fixed. The essential difference between our steady state analysis and their experiment concerns the geometry of the membrane. The essential similarity, and that which dominates the comparison, is that the driving force for the film flow—the thermomolecular pressure gradient—is the same.

VI. DISCUSSION

We have studied the basic mechanisms associated with the transport of interfacially premelted films under the force of thermomolecular pressure gradients using a simple model of solidification inside a capillary tube. Our analysis is valid for any material that undergoes interfacial premelting in the mean-field sense outlined, which includes nonretarded van der Waals forces, and other effects which result in a power law dependence like that in Eq. (7). Interactions which are stronger than van der Waals may still be modeled as we have done, but by varying the strength through the coefficient λ. By imposing a temperature gradient parallel to the premelted interface, a thermomolecular pressure gradient drives unfrozen liquid towards lower temperatures. Material in excess of the equilibrium thickness [Eq. (7)] at any position along the interface solidifies and the membrane confining the fluid layer distorts. We have derived and solved the relevant field equations for transient and steady state temperature gradients. The latter solution is relevant to, and in

qualitative agreement with, experiments using pure H_2O ice [21]. We find a marked distinction between the shapes of membrane deformation in the two cases. In the transient case there is primary deformation in a thin boundary near the bulk solid-liquid interface which relaxes to a *small* constant value at low temperatures. In the fixed gradient case most of the deformation occurs near the bulk solid-liquid interface and creates the bulge shown in Fig. 3, which migrates away from the bulk interface at a rate proportional to $t^{-2/3}$. The simple model we have studied elucidates some of the underlying dynamics of frost-heave phenomena in model porous media and in natural soils.

As the temperature is lowered the liquid layer thins, its entropy density decreases, and this results in a solid-like ordering in the film. Therefore, two important effects occur at low temperatures: the viscosity increases relative to the bulk value, and the continuum approximation begins to break down. An experimental deduction of the film thickness requires an estimation of the viscosity [21]; hence we have a unique, although indirect, opportunity to study proximity induced ordering adjacent to interfaces in terms of dynamical quantities. New microscopic and semimicroscopic models of fluid viscosity can then be tested. Another issue of proximity concerns the role of corrugations in wetting and surface melting, which has been investigated in static cases [29]. Dynamic aspects of these problems may be addressed using a geometrically disordered capillary. In addition, proximity effects in quantum systems, such as helium, might be examined in a qualitatively similar manner.

There are two situations of great practical importance where our analysis may be of use: geophysical and biological. Since frost heave is responsible for damage to engineered structures, the breakdown of rock [30], and for the creation of regular geomorphological features [3,11], we anticipate that our "local" dynamics could be brought to bear on porous media problems. Although curvature and impurity effects may dominate the dynamics, water transport along veins between crystal grains, grain coarsening, and the ablation of glacier ice are situations that are also related to our study [31].

The dynamical concepts we have presented may help in understanding the freezing of biological cells, either for tissue preservation, medical treatment, food science, or fish biology. Both phase change problems involving ice and ordering of water at membrane walls have been actively studied (e.g., [32]). If frozen in a transient thermal field our results suggest small uniform deformation, but the steady field will eventually create large deformations which may not be reversible. Hence frost-heave damage can be minimized in a transient thermal field.

Finally, it is generally not appreciated that in most cases films are *formed* under conditions *out* of equilibrium. Since the thermomolecular pressure gradient is only present in a temperature gradient, this approach provides information not available in isothermal experiments. The correspondence between the liquid-gas system and magnetic systems (e.g., [1]) suggests a potential link between the present analysis and the dynamics of systems with long range interactions whose critical behavior can be described by mean-field theory. Our approach should be useful in the study of (a) the dynamics of thin films wherein one interface is *free*, e.g., surface melting or gas-liquid wetting on a substrate and (b) shape *transitions* during phase separation of a binary liquid [6(a)] in a pore. Thus thermomolecular pressure and the associated transport offer a tool for fundamental physics research on a variety of systems and provide new insights on problems of practical importance.

ACKNOWLEDGMENTS

The authors wish to thank J. G. Dash, M. Elbaum, H.-Y. Fu, and L. Wilen for their comments and criticisms, and continually enlightening conversations. J.S.W. acknowledges the hospitality of ITG/DAMTP, Cambridge University, and the support of ONR under Grants No. N00014-93-J-1369, No. N00014-94-1-0120, and No. APL/UW. M.G.W. is supported by the NERC and by a grant from the Microgravity Science and Applications Division of NASA.

APPENDIX

We collect here a number of the similarities between the interfacial thermodynamics presented in Sec. II, and the approaches which are more common to those used in wetting phenomena. The point is to show that different approaches are related in a straightforward manner. More complete, albeit different treatments are given by Schick [1] and Israelachvili [24], and the dynamics of wetting is treated by deGennes, and Leger and Joanny [19].

We begin by showing how the form of the interfacial term appearing in Eq. (1) arises from a simple treatment. Considering only nonretarded van der Waals interactions, Israelachvili [24] shows that the interfacial energy of an isolated interface, γ, is half the adhesion energy $\frac{A}{24\pi\sigma^2}$, where A is the Hamaker constant and σ, as in our treatment, is of order a molecular diameter. We can derive our expression by generalizing his argument to consider two interfaces separating different materials a distance d apart. The total interfacial free energy per unit area is

$$I_T = \frac{A_{s\ell}}{24\pi\sigma^2} + \frac{A_{\ell w}}{24\pi\sigma^2} - \frac{A_{sw}}{12\pi d^2}. \tag{A1}$$

As $d \to \infty$,

$$I_T \to \frac{A_{s\ell} + A_{\ell w}}{24\pi\sigma^2} \equiv \gamma_{s\ell} + \gamma_{\ell w}, \tag{A2}$$

and as $d \to \sigma$,

$$I_T \to \gamma_{s\ell} + \gamma_{\ell w} - \frac{A_{sw}}{12\pi\sigma^2} \equiv \tilde{\gamma}_{sw}, \tag{A3}$$

where $\tilde{\gamma}_{sw}$ is the nonequilibrium quantity that we *would* measure *if* we *could* bring the wall up to the solid without the formation of a melt layer. By definition, $\Delta\gamma = \gamma_{s\ell} + \gamma_{\ell w} - \tilde{\gamma}_{sw}$, so that $\frac{A_{sw}}{12\pi} = \sigma^2\Delta\gamma$, and hence we obtain

$$I_T = \Delta\gamma f(d) + \tilde{\gamma}_{sw}, \tag{A4}$$

which is our $\mathcal{I}(d)$ per unit area. Schick [1] derives the quantity analogous to $\tilde{\gamma}_{sw}$ for the vapor-liquid-wall system as an integral equation over the interaction potentials, and also shows that the *equilibrium* wall-vapor coefficient γ_{wv} can never exceed the sum of the wall-liquid and liquid-vapor coefficients, $\gamma_{w\ell} + \gamma_{\ell v}$. If a measured quantity does so, then it is analogous to $\tilde{\gamma}_{sw}$ above, and represents the nonequilibrium value. This, of course, is directly relevant to the wetting of volatile and nonvolatile liquids on substrates. In the latter sytems, the "dry" interfacial coefficient is, in principle, a measurable quantity, but in all of these cases $\Delta\gamma$ is a measure of the *drive* toward equilibrium, and hence $\mathcal{I}(d)$ is an effective interfacial interaction. Therefore the total interfacial energy can be viewed as a perturbation of the surface free energies with the film thickness dependence given by $f(d)$. Finally, the so-called *spreading parameter* S of de Gennes [19] is just $-\Delta\gamma$. (S is not to be confused with the Stefan number used in Sec. IV.)

As shown above, $\frac{A_{sw}}{12\pi} = \sigma^2\Delta\gamma$, so that one can rewrite the thermodynamic results of Sec. II in equally useful forms using these substitutions:

$$\sigma^2\Delta\gamma = \frac{A_{sw}}{12\pi} = -\sigma^2 S. \tag{A5}$$

[1] M. Schick, in *Liquids at Interfaces*, Proceedings of the Les Houches Summer School of Theoretical Physics, Session XLVIII, Haute-Savoie, 1988, edited by J. Charvolin, J.F. Joanny, and J. Zinn-Justin (Elsevier, Amsterdam, 1990), pp. 415–498.

[2] H. Löwen, T. Beier, and H. Wagner, Europhys. Lett. **9**, 791 (1989); R. Lipowsky, U. Breuer, K.C. Prince, and H.P. Bonzel, Phys. Rev. Lett. **62**, 913 (1989); H. Löwen, Phys. Rep. **237**, 249 (1994).

[3] J.G. Dash, J. Low Temp. Phys. **89**, 277 (1992); J.G. Dash, H.-Y. Fu, and J.S. Wettlaufer, Rep. Prog. Phys. **58**, 115 (1995).

[4] E. Cheng and M.W. Cole, Phys. Rev. B **41**, 9650 (1990); M. Napiórkowski, W. Koch, and S. Dietrich, Phys. Rev. A **45**, 5760 (1992); E.H. Hauge, *ibid.* **46**, 4994 (1992).

[5] For a review, see R. Evans, J. Phys. Condens. Matter **2**, 8989 (1990). For a recent model study see M.R. Swift, E. Cheng, M.W. Cole, and J.R. Banavar, Phys. Rev. B **48**, 3124 (1993).

[6] (a) A.J. Liu, D.J. Durian, E. Herbolzheimer, and S.A. Safran, Phys. Rev. Lett. **65**, 1897 (1990); (b) A.J. Liu and G.S. Grest, Phys. Rev. A **44**, R7894 (1991); (c) L. Monette, A.J. Liu, and G.S. Grest, *ibid.* **46**, 7664 (1992).

[7] S. Dietrich, Phys. Scr. **T49B**, 519 (1993).

[8] (a) J.G. Dash, in *Proceedings of the Nineteenth Solvay Conference,* edited by F.W. de Wette (Springer-Verlag, Berlin, 1988); (b) S. Dietrich, in *Phase Transitions and Critical Phenomena*, edited by C. Domb and J. Lebowitz (Academic, New York, 1988), Vol. 12; (c) J.G. Dash, Contemp. Phys. **30**, 89 (1989).

[9] J.W. Cahn, J.G. Dash, and H.-Y. Fu, J. Cryst. Growth **123**, 101 (1992); J.M. Gay, J. Suzanne, J.G. Dash, and H.-Y. Fu, *ibid* **125**, 33 (1992).

[10] H.-Y. Fu and J.G. Dash, J. Colloid Interface Sci. **159**, 343 (1993).

[11] J.G. Dash, in *Phase Transitions in Surface Films*, Vol. 267 of *NATO Advanced Study Institute, Series B: Physics,* edited by H. Taub, S.C. Fain, Jr., G. Torzo, and H.J. Lauter (Plenum, New York, 1991); Science **246**, 1591 (1989).

[12] Y. Furukawa and I. Ishikawa, J. Cryst. Growth **128**, 1137 (1993).

[13] (a) R.R. Gilpin, J. Colloid Interface Sci. **77**, 435 (1980); (b) Water Resour. Res. **16**, 918 (1980).

[14] M. Elbaum and M. Schick, Phys. Rev. Lett. **66**, 1713 (1991); R. Bar-Ziv and S.A. Safran, Langmuir **9**, 2786 (1993); L. Wilen, J.S. Wettlaufer, M. Elbaum, and M. Schick (unpublished).

[15] M. Elbaum, S.G. Lipson, and J.G. Dash, J. Cryst. Growth **129**, 491 (1993).

[16] R. Kukuchi and J.W. Cahn, Phys. Rev. B **21**, 1893 (1980); O.G. Mouritsen and M.J. Zuckermann, Phys. Rev. Lett. **58**, 389 (1987).

[17] M. Schick and Wei-Heng Shih, Phys. Rev. B **35**, 5030 (1987).

[18] J.Q. Broughton and G.H. Gilmer, Phys. Rev. Lett. **56**, 2692 (1986).

[19] (a) P.G. de Gennes, Rev. Mod. Phys. **57**, 827 (1985); (b) J.N. Israelachvili, Surf. Sci. Rep. **14**, 109 (1992); (c) L. Leger and J.F. Joanny, Rep. Prog. Phys. **55**, 431 (1992).

[20] M.W. Cole and W.F. Saam, Phys. Rev. Lett. **32**, 985 (1974); J.-M. di Meglio, D. Quéré, and F. Brochard-Wyart, C. R. Acad. Sci. **309 II**, 19 (1989).

[21] L. Wilen and J.G. Dash, Bull. Am. Phys. Soc. **38**, 747 (1993); Phys. Rev. Lett. (to be published).

[22] B.V. Derjaguin and N.V. Churaev, Cold Reg. Sci. Technol. **12**, 57 (1986).

[23] M. Vignes and K.M. Dijkema, J. Colloid Interface Sci. **49**, 165 (1974); M. Vignes-Adler, *ibid.* **60**, 162 (1977).

[24] J.N. Israelachvili, *Intermolecular and Surface Forces* (Academic, New York, 1992). Also, see the Appendix.

[25] Note that we are free to expand μ_j about any point on the T, P solid-liquid coexistence line. However, as will be seen, the interesting behavior is in the region of small reduced temperature, so we expand about T_m, P_m.

[26] L.D. Landau and I.M. Lifshitz, *Fluid Mechanics* (Pergamon, New York, 1958).

[27] H.S. Carslaw and J.C. Jaeger, *Conduction of Heat in Solids* (Clarendon, Oxford, 1986). Stefan originally studied the growth of floating ice, but a general class of free boundary solidification problems goes by this name.

[28] E.J. Hinch, *Perturbation Methods* (Cambridge University Press, Cambridge, England, 1991).

[29] D. Andelman, J.F. Joanny, and M.O. Robbins, Europhys. Lett. **7**, 731 (1988) (wetting); R.R. Netz and D. Andelman (unpublished); and D. Beaglehole and P. Wilson, J. Phys. Chem. **98**, 8096 (1994) (interfacial melting).

[30] J. Walder and B. Hallet, Geol. Soc. Am. Bull. **96**, 336 (1985).

[31] J.F. Nye, in *Physics and Chemistry of Ice,* edited by N. Maeno and T. Hondoh (Hokkaido University Press, Sapporo, 1992), p. 200.

[32] V.A. Parsegian, in *Physical Chemistry: Enriching Topics from Colloid and Surface Science,* edited by H. van Olphen and K.J. Mysels (Theorex, La Jolla, CA, 1975), p. 25.